Giant energy density in [001]-textured Pb(Mg1/3Nb2/3)O3-PbZrO3-PbTiO3 piezoelectric ceramics

Yongke Yan, Kyung-Hoon Cho, Deepam Maurya, Amit Kumar, Sergei Kalinin, Armen Khachaturyan, and Shashank Priya

Citation: Applied Physics Letters **102**, 042903 (2013); doi: 10.1063/1.4789854
View online: http://dx.doi.org/10.1063/1.4789854
View Table of Contents: http://scitation.aip.org/content/aip/journal/apl/102/4?ver=pdfcov
Published by the AIP Publishing

Giant energy density in [001]-textured $Pb(Mg_{1/3}Nb_{2/3})O_3$-$PbZrO_3$-$PbTiO_3$ piezoelectric ceramics

Yongke Yan,[1] Kyung-Hoon Cho,[1] Deepam Maurya,[1] Amit Kumar,[2] Sergei Kalinin,[2] Armen Khachaturyan,[3] and Shashank Priya[1,a)]
[1]*Bio-Inspired Materials and Devices Laboratory (BMDL), Center for Energy Harvesting Materials and Systems (CEHMS), Virginia Tech, Virginia 24061, USA*
[2]*Oak Ridge National Laboratory, Oak Ridge, Tennessee 37831, USA*
[3]*Rutgers, The State University of New Jersey, Piscataway, New Jersey 08854, USA*

(Received 10 December 2012; accepted 15 January 2013; published online 28 January 2013)

$Pb(Zr,Ti)O_3$ (PZT) based compositions have been challenging to texture or grow in a single crystal form due to the incongruent melting point of ZrO_2. Here we demonstrate the method for achieving 90% textured PZT-based ceramics and further show that it can provide highest known energy density in piezoelectric materials through enhancement of piezoelectric charge and voltage coefficients (d and g). Our method provides more than $\sim 5\times$ increase in the ratio d(textured)/d(random). A giant magnitude of $d{\cdot}g$ coefficient with value of $59\ 000 \times 10^{-15}\ m^2\ N^{-1}$ (comparable to that of the single crystal counterpart and 359% higher than that of the best commercial compositions) was obtained. © *2013 American Institute of Physics*. [http://dx.doi.org/10.1063/1.4789854]

Conversion of mechanical energy to electrical energy or vice-versa (electromechanical coupling effect) through piezoelectric materials provides a wide range of transducer applications.[1] The performance of piezoelectric materials for mechanical to electrical conversion is generally characterized by piezoelectric charge/strain coefficient d and piezoelectric voltage coefficient g,[1] since the energy density (e) for piezoelectric is defined as $e = \frac{1}{2}(d \cdot g) \cdot \left(\frac{F}{A}\right)^2$, where F is the applied force and A is the area of active piezoelectric material.[2,3] Since the discovery of $Pb(Zr,Ti)O_3$ (PZT) system exhibiting morphotropic phase boundary (MPB) in the mid 1950s,[4] many investigations on developing high performance piezoelectric materials have been conducted. Defects and substituents have been used to modify the electromechanical properties of the ceramics in poled conditions. However, the success through these doping methods has been limited. As shown in Fig. 1(a), commercialized PZT compositions exhibiting either high d_{33} value or high g_{33} value can be found,[5] but not both at the same time. As seen in Fig. 1(a), the $d_{33}{\cdot}g_{33}$ values of commercialized piezoelectric ceramics are confined below 16500×10^{-15} $m^2\ N^{-1}$. This is fundamental limitation imposed by the thermodynamics constraints. Using Landau–Devonshire theory, the energy due to the fluctuations in the polarization p and strain u can be written as $f = \frac{1}{2\chi^u}p^2 + apu + \frac{1}{2}c^p u^2$, where χ^u is the susceptibility under constant strain, a is the piezoelectric coefficient relating the polarization and strain, and c^p is the elastic stiffness under constant polarization. For simplicity, only one polarization and one strain component were considered in the above expression. The derivative of polarization with respect to the applied stress X can be written as $dp/dX = -as\chi + higher\ order\ terms$, where s is the elastic compliance. This implies that any increase in the piezoelectric constant is always accompanied by the increase in transversal dielectric susceptibility and thus the product ($d{\cdot}g$) is almost constant.[6]

As depicted in Figs. 2(a) and 2(b), the electromechanical properties of piezoelectric materials can be improved by utilizing the intrinsic anisotropy. It is well-known that ⟨001⟩ oriented relaxor-based piezoelectric single crystals such as $Pb(Mg_{1/3}Nb_{2/3})O_3$–$PbTiO_3$ (PMN-PT) and $Pb(Zn_{1/3}Nb_{2/3})O_3$–$PbTiO_3$ (PZN-PT) with rhombohedral structure near MPB exhibit $d_{33} > 2000\ pC\ N^{-1}$ and $k_{33} > 92\%$.[6] These giant piezoelectric properties of ⟨001⟩ rhombohedral crystals are related to their piezoelectric anisotropy and "engineered domain states" that facilitate the rotation of ⟨111⟩ polarization toward the ⟨001⟩ direction.[7,8] Figure 2(d) shows the schematic diagram of unit cell of ABO_3 perovskite structure. Corner metal ions (green balls) are in A-site, and center metal ion in oxygen octahedron occupies B-site. Yellow dotted arrows indicate directions of equivalent ⟨111⟩ spontaneous polarizations in rhombohedral perovskite ferroelectrics after the poling process. The domain configurations consisting of these equivalent ⟨111⟩ polarizations exhibit high piezoelectric response along the ⟨001⟩ direction and is often called engineered domain state.

The first principle calculations have demonstrated a significant reduction of dipolar anisotropy associated with an existence of tetragonal and rhombohedral polymorphs. This results in large piezoelectric strain due to the ease of polarization rotation caused by the existence of these polymorphs as well as the large crystal lattice misfit between the polymorphs.[8] It has also been shown that the reduction of the dipolar anisotropy is a quite generic thermodynamic property of the ferroelectric solid solutions near MPB separating the rhombohedral and tetragonal phases on the diffusion-less phase diagram.[9,10] Fig. 2(f) displays the angular dependence of the energy of dipolar anisotropy for the generic PZT MPB system. This figure illustrates a gradual compositional transformation of the geometry of the dipolar anisotropy from the one providing the minima at the ⟨111⟩ directions that stabilizes the rhombohedral phase to the geometry providing the minima at the ⟨100⟩ directions that stabilizes the tetragonal phase. A point of the transition between these geometries,

a)E-mail: spriya@vt.edu.

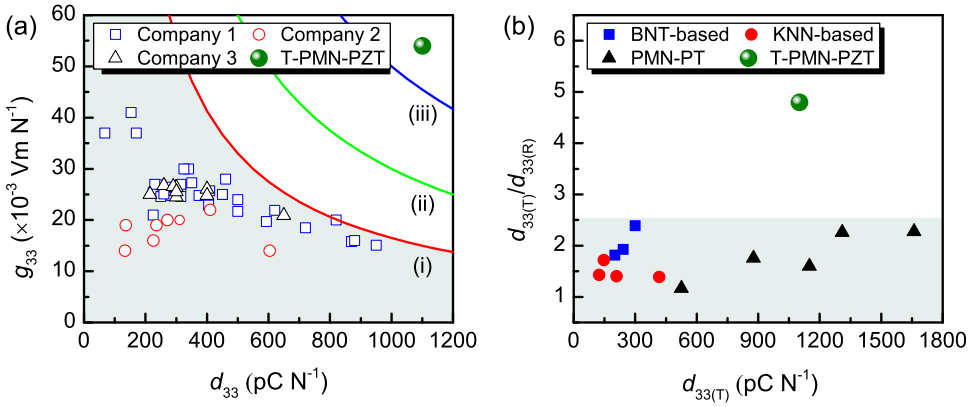

FIG. 1. (a) Comparison of g_{33} and d_{33} values of various piezoelectric ceramics (Ref. 5). Different colored lines (i), (ii), and (iii) indicate the plots of $g_{33}{\cdot}d_{33} = c$ function; (i) $c = 16500 \times 10^{-15}\,m^2\,N^{-1}$, (ii) $c = 30\,000 \times 10^{-15}\,m^2\,N^{-1}$, and (iii) $c = 50\,000 \times 10^{-15}\,m^2\,N^{-1}$. (b) Comparison of $d_{33(T)}/d_{33(R)}$ ratio vs. $d_{33(T)}$ of various textured piezoelectric ceramics. The $d_{33(T)}$ and $d_{33(R)}$ represent d_{33} of textured ceramic and that of randomly oriented counterpart, respectively. BNT and KNN represent $(Bi_{1-x}Na_x)TiO_3$ and $(K_{1-x}Na_x)NbO_3$ compositions, respectively.

the composition, c_{MB}, corresponds to the MPB. At this composition the shape becomes spherical, i.e., the dipolar anisotropy vanishes.[9,10]

Although domain engineered relaxor piezoelectric single crystals have been grown to achieve high performance, low ferroelectric rhombohedral to tetragonal phase transition temperature ($T_{R\text{-}T} \sim 60$–$90\,^{\circ}C$), and low coercive fields ($E_C \sim 2$–3 kV cm^{-1}) limit the stability of electrical property in relaxor-based single crystals.[11] Many attempts to grow PZT-based single crystals near MPB to achieve high and stable piezoelectric properties have been made, but there is a fundamental challenge in accomplishing this task.[12] The PZT solid solution presents congruent melting point only for the end-component of PT phase. For other compositions and, particularly, near the MPB, melting is incongruent and results in the precipitation of zirconia prior to the formation of PZT. Thus any effort to grow MPB composition single crystal using liquid phase results in a mixture consisting of zirconia and Zr-deficient PZT grains.

Here we adopted a very different strategy for overcoming the fundamental limitations imposed by electrodynamics and thermodynamics. We demonstrate template grain growth (TGG) technique that yields microstructure which surpasses the ($d{\cdot}g$) magnitude of even single crystals. Using this technique, we achieved two goals: (1) ⟨001⟩ texturing (grain orientation along the ⟨001⟩ crystallographic direction) of piezoelectric ceramic (Fig. 2(c)) with engineered domain state similar to that of ⟨001⟩ single crystals to obtain high d values, and (2) realization of high $d{\cdot}g$ coefficient by suppressing the ε^T of textured piezoelectric ceramic through the use of low ε^T templates.

In TGG process, template crystals are aligned in ceramic matrix powder by tape-casting process.[13–16] During the high

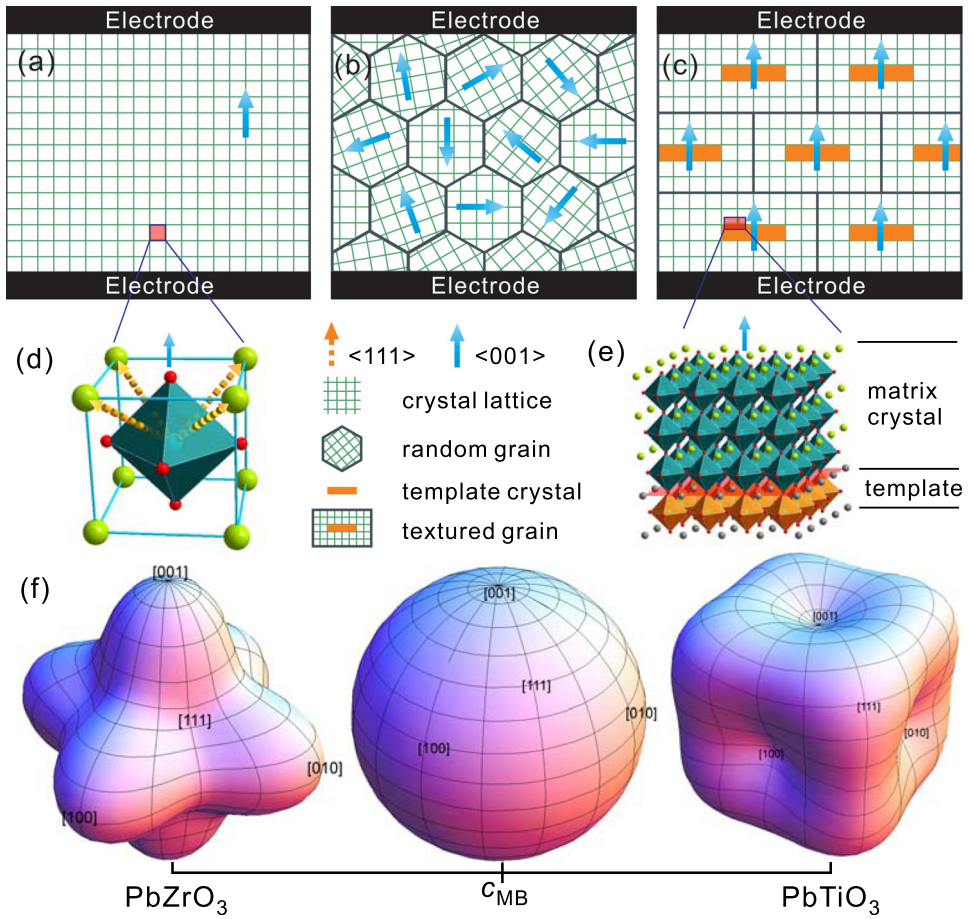

FIG. 2. Schematic diagram of (a) ⟨001⟩ oriented single crystal, (b) randomly oriented polycrystalline ceramic, and (c) ⟨001⟩ textured polycrystalline ceramic. Blue arrow indicates ⟨001⟩ crystallographic direction of crystal lattice. (d) Schematic diagram of unit cell of ABO_3 perovskite structure. (e) Schematic diagram of grown matrix crystal on surface of perovskite template crystal. (f) An angular dependence of the energy of dipolar anisotropy for the generic PZT morphotropic system.

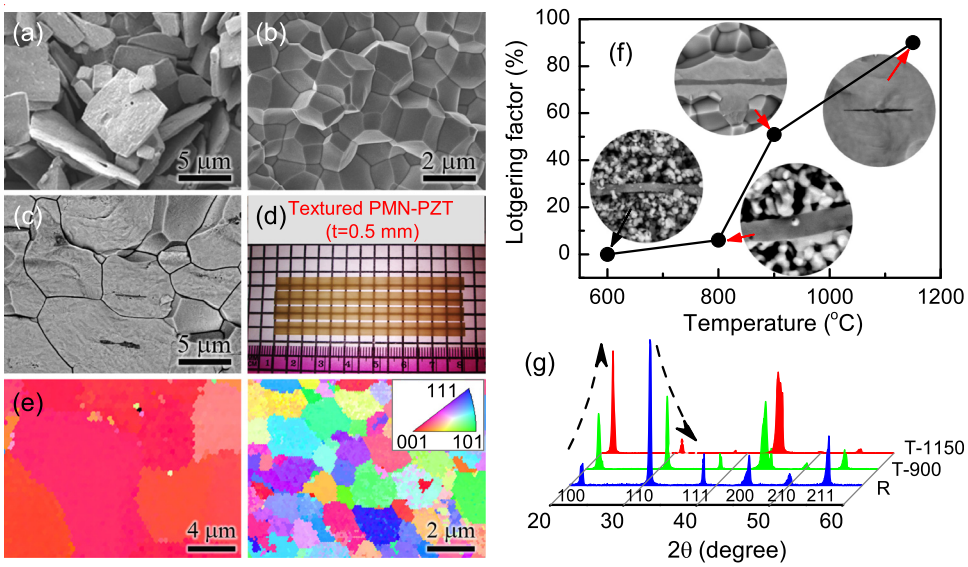

FIG. 3. SEM images of (a) BT template crystals, (b) fractured random PMN-PZT, and (c) fractured textured PMN-PZT. (d) Photograph of long (70 mm) textured PMN-PZT ceramics strip. (e) EBSD inverse pole figure maps using stereographic projection of textured (left) and random (right) PMN-PZT ceramics. (f) ⟨001⟩ Lotgering factors of textured PMN-PZT samples sintered at various temperatures for 2 h. Inset SEM images show the evolution of matrix PMN-PZT crystal growth on BT template crystal with variation of sintering temperature. (g) XRD patterns of random and textured PMN-PZT samples. R and T-1150 denote the random and textured sample sintered at 1150 °C, respectively, and T-900 denotes the textured sample sintered at 900 °C.

temperature sintering process, the powder compact undergoes fast densification. After a specific density level (>95%) has been achieved, the nucleation and growth of matrix crystals on the aligned template crystals starts to dominate the sintering process and drives the enhancement in texturing degree.[12] The template crystals should possess a thin platelet morphology with {001} plane to facilitate their homogeneous alignment in the matrix and interfacial growth along the ⟨001⟩ direction (Fig. 2(e)). Rhombohedral composition given as $0.4Pb(Mg_{1/3}Nb_{2/3})O_3$-$0.25PbZrO_3$-$0.35PbTiO_3$ (PMN-PZT) was used as matrix because its ⟨001⟩ single crystal counterpart shows excellent piezoelectric properties ($d_{33} = 1530\,pC\,N^{-1}$, $k_{33} = 0.93$) and much better thermal and electrical stabilities ($T_C = 211\,°C$ and $E_C = 4.5\,kV\,cm^{-1}$) than those of PMN-PT or PZN-PT crystals ($T_C = 130$–$170\,°C$ and $E_C = 2$–$3\,kV\,cm^{-1}$).[17,18] We selected $BaTiO_3$ (BT) as template due to its chemical stability in PMN-containing ceramics[13–16] and good lattice match with the PMN-PZT composition (lattice parameter: ~4.05 Å). Moreover, we took notice of the low relative permittivity of ⟨001⟩ BT crystal ($\varepsilon_{33}^T/\varepsilon_0 = 130$, ε_0: vacuum permittivity).[19]

The composition of PMN-PZT was synthesized by conventional solid state reaction. Compositionally pure BT template crystals with desired morphology (dimension: ~10 μm × 10 μm × 0.5 μm) were synthesized by topochemical microcrystal conversion (TMC) method as shown in Fig. 3(a).[20] After embedding the 5 vol. % BT template crystals, the PMN-PZT ceramic was sintered at different temperatures for 2–10 h. The processing details can be found in the Ref. 5. Compared to the randomly oriented ceramic in Fig. 3(b)), a highly textured sample in Fig. 3(c) was developed with a brick wall-like structure. Electron backscatter diffraction (EBSD) mapping images in Fig. 3(e) directly demonstrate that the textured sample has strong ⟨001⟩ preferred orientation while the random sample has no preferred orientation. The texture development and microstructure evolution are clearly shown in Figs. 3(f) and 3(g). The Lotgering factor implying ⟨001⟩ texture degree was calculated by using X-ray diffraction (XRD) peaks of sintered specimens. At the sintering temperature of 600 °C, the matrix PMN-PZT particles were observed to surround the BT template without any growth in the matrix. The nucleation and growth on the surface of BT template initiated around 800 °C for 2 h, and interface migration was observed from the sample sintered at 900 °C for 2 h. High ⟨001⟩ Lotgering factor of 90% with highly textured microstructure was obtained from the specimen sintered at 1150 °C for 10 h. XRD patterns in Fig. 3(g) show that the intensity of {001} peaks in the textured sample is increased while that of other peaks is decreased with increasing sintering temperature. This change in the relative peak heights shows an enhanced degree of texture. Unlike single crystal synthesis (high cost, small crystal size, etc.), large textured specimens with a length of ~7 cm were easily fabricated as shown in Fig. 3(d).

Table I summarizes the piezoelectric and dielectric properties of randomly oriented ceramic (R-ceramic), ⟨001⟩ textured ceramic (T-ceramic), and ⟨001⟩ single crystal (S-crystal) of PMN-PZT composition. T-ceramic exhibited giant d_{33} of 1100 pC N^{-1} which is 4.8 times higher than that of R-ceramic (230 pC N^{-1}). This increasing ratio of d_{33} value between R- and T-ceramic (4.8) was much higher than that of the other textured piezoelectric ceramics (usually less than 2.5) as shown in Fig. 1(b). Highly enhanced d_{33} of T-ceramic is also evidenced by strain vs. electric field characteristic in Fig. 4(a). Compared to R-ceramic, T-ceramic exhibited much higher strain value (0.24% at 20 kV cm^{-1}) proving the high strain coefficient and demonstrating its

TABLE I. Piezoelectric and dielectric properties of PMN-PZT: randomly oriented ceramic (R-ceramic), ⟨001⟩ textured ceramic (T-ceramic), and ⟨001⟩ single crystal (S-crystal).

Properties	R-ceramic	T-ceramic	S-crystal[a]
d_{33} (pC N^{-1})	230	1100	1530
K	0.4 (k_p)	0.84 (k_p)	0.93 (k_{33})
$\varepsilon_{33}/\varepsilon_0$	915	2310	4850
g_{33} (×10^{-3} V m N^{-1})	28.4	53.8	35.6
$d_{33}\cdot g_{33}$ (×10^{-15} m^2 N^{-1})	6532	59180	54468
P_r (μC cm^{-2})	30	36	29
E_c (kV cm^{-1})	8.2	7.4	4.5
T_c (°C)	233	204	211

[a]Reference 18.

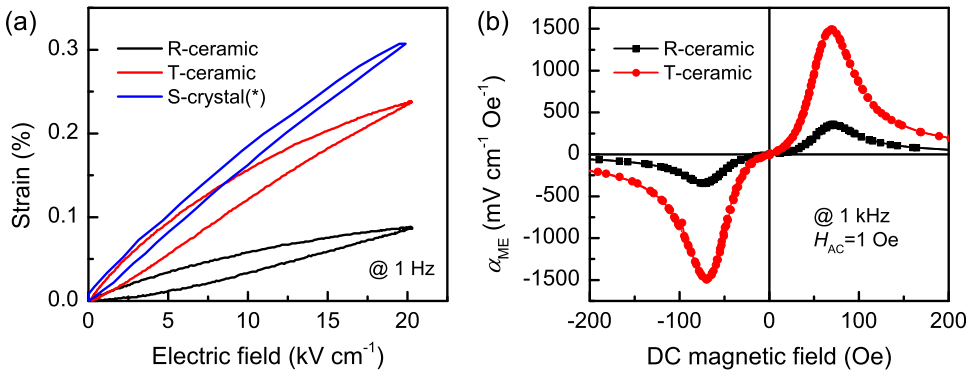

FIG. 4. (a) Strain vs. electric field curves of randomly oriented ceramic (R-ceramic), ⟨001⟩ textured ceramic (T-ceramic), and ⟨001⟩ single crystal (S-crystal). (b) Magentoelectric (ME) voltage coefficients (α_{ME}) of random and textured PMN-PZT ceramics.

superior feasibility for actuator applications. Planar mode coupling coefficient (k_p) of T-ceramic was found to be more than 2 times higher than that of R-ceramic. The most notable point is that via ⟨001⟩ texturing the permittivity value was increased by only 2.5 times while the d_{33} was increased by 4.8 times. This suppressed permittivity value of T-ceramic resulted in very high g_{33} of 53.8×10^{-3} V m N^{-1} (even much higher than S-crystal value). High g_{33} of T-ceramic obtained by high d_{33} and suppressed permittivity yielded a giant transduction coefficient of 59180×10^{-15} m^2 N^{-1} which is 9 times higher than that of R-ceramic and even higher than S-crystal value.

To clearly show the advantage of high d, k, g with low ε in textured ceramic, ME laminate composite was fabricated in the form of three-layer structure corresponding to Metglas (2605SA1, Metglas Inc., USA)/textured PMN–PZT/Metglas. Sample preparation, fabrication, and characterization details of ME composite can be found elsewhere.[5,21] Fig. 4(b) shows the ME coefficients (α_{ME}) of random and textured PMN-PZT laminates where the maximum was found to be 348 mV cm^{-1} Oe^{-1} and 1490 mV cm^{-1} Oe^{-1}, respectively. The 3.4 times improvement of α_{ME} could be explained on the basis of the textured microstructure.

Giant piezoelectric response of textured PMN-PZT ceramic can be understood by noticing the role of special microstructure where BT templates are embedded in the matrix grains. The BT template inclusions have comparatively high polar anisotropy suppressing rotation of its polarization under applied electric field. This is contrary to the properties of the matrix phase, PMN-PZT, that being near MPB, has a drastically reduced polar anisotropy.[9,10] In this scenario, the PMN-PZT matrix can be regarded as "soft ferroelectric" under the constant electric and stress fields imposed on this matrix by the presence of BT inclusions. These electric and stress fields are generated by both fixed polarization of the BT template inclusions and crystal lattice misfit between the phases, which in turn depends on the morphology, orientation relations with the matrix, and polarization. Given the low polar anisotropy of the PMN-PZT matrix, a direction of its energy-minimizing polarization is determined by the coupling with the BT-generated fixed electric and stress fields imposed on the matrix. Application of the external electric field produces a deviation in the polarization direction of the PMN-PZT matrix from its energy minimizing direction. This deviation produces the dielectric and strain response that are significant due to the "soft" character of the matrix. A lifting of the applied electric field reverses the deviation and results in the recovery of the initial energy-minimizing polarization direction. This reversal caused by the coupling with the template-generated constant fields is practically hysteresis-free. Therefore, the polar anisotropy of the PMN-PZT in this two-phase composite is determined by the interaction of the polarization of the PMN-PZT with the local static electric and stress fields generated by the BT rather than by the intrinsic properties of the PMN-PZT. This coupling together with the low polar anisotropy of the PMN-PZT results in maximum piezoelectric strain inherent to the PMN-PZT with the enhancement of blocking force caused by electrostatic and stress-induced interaction between the phases. The discovered processing regime providing a composite with very high texture of the PMN-PZT grains—this is a state that is close to the PMN-PZT single crystal with oriented BT inclusions—is the important factor that results in high energy density.

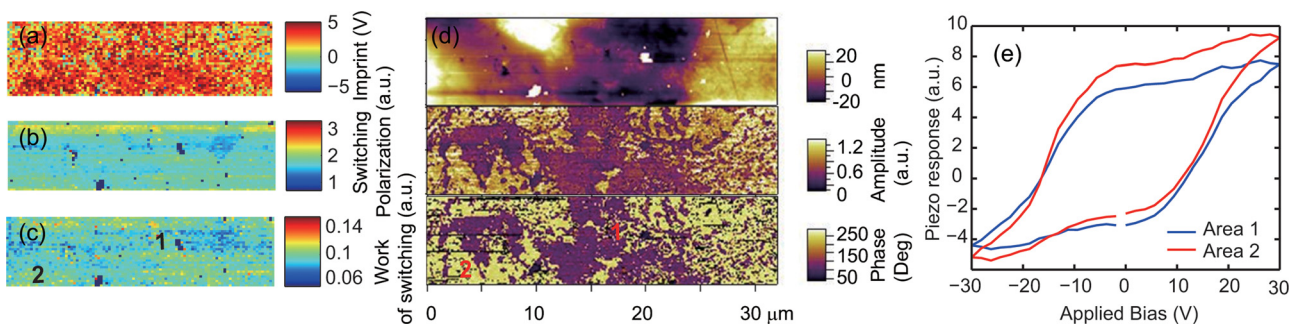

FIG. 5. Local switching properties across the templated region in PMN-PZT sample. (a) Imprint (horizontal offset), (b) switching polarization (loop height), (c) work of switching (loop area), (d) piezoelectric response, and (e) selected local hysteresis loops.

The local switching characteristics across the templated region with the embedded BT phase were studied using switching spectroscopy PFM technique. Local hysteresis loops were collected across a 40×100 matrix which contains the BT phase as well as the PMN-PZT matrix, and switching parameters like imprint, switching polarization, and work of switching were mapped across the surface (Fig. 5). The hysteresis loops opened more in the matrix (area 2) in comparison to the BT template (area 1), and the local switching behavior across the textured samples was in conformity with the macroscopic switching behavior. These results further confirmed that the texturing enhances the homogeneity of the polarization across the matrix which thereby provides an additive effect promoting the low polar anisotropy. It also validates our hypothesis that the interaction between the polarization and local fields generated in the vicinity of BT play an important role towards controlling the global response.

In summary, the results presented here clearly demonstrate that $\langle 001 \rangle$ textured PMN-PZT ceramics can provide the highest $d_{33} \cdot g_{33}$ coefficient among reported values of polycrystalline piezoelectric ceramics to date. We believe this result will open new piezoelectric application areas in addition to strengthening the piezoelectric energy harvesting investigations.

We gratefully acknowledge the financial support from DARPA Heterostructural Uncooled Magnetic Sensors (HUMS Program) (Y.Y. and K.C.) and Office of Basic Energy Science, Department of Energy through DE-FG02-07ER46480 (D.M. and S.P.). A.M. was supported through the grant DE-FG02-08ER46484. PFM analysis was conducted at the Center for Nanophase Materials Science, Oak Ridge National Laboratory by the Scientific User Facilities Division, U.S. Department of Energy.

[1]K. Uchino, *Ferroelectric Devices*, 2nd ed. (CRC, 2010).
[2]R. A. Islam and S. Priya, Appl. Phys. Lett. **88**, 032903 (2006).
[3]S. Priya, IEEE Trans. Ultrason. Ferroelectr. Freq. Control **57**, 2610 (2010).
[4]B. Jaffee, R. S. Roth, and S. Marzullo, J. Appl. Phys. **25**, 809 (1954).
[5]See supplementary material at http://dx.doi.org/10.1063/1.4789854 for experimental procedure and reference list of Fig. 1.
[6]Y. Ishibashi and M. Iwata, Jpn. J. Appl. Phys., Part 1 **38**, 800 (1999).
[7]S. E. Park and T. R. Shrout, J. Appl. Phys. **82**, 1804 (1997).
[8]H. X. Fu and R. E. Cohen, Nature (London) **403**, 281 (2000).
[9]G. A. Rossetti, A. G. Khachaturyan, G. Akcay, and Y. Ni, J. Appl. Phys. **103**, 114113 (2008).
[10]A. G. Khachaturyan, Philos. Mag. **90**, 37 (2010).
[11]S. J. Zhang and F. Li, J. Appl. Phys. **111**, 031301 (2012).
[12]R. Clarke and R. W. Whatmore, J. Cryst. Growth **33**, 29 (1976).
[13]G. L. Messing, S. Trolier-McKinstry, E. M. Sabolsky, C. Duran, S. Kwon, B. Brahmaroutu, P. Park, H. Yilmaz, P. W. Rehrig, K. B. Eitel, E. Suvaci, M. Seabaugh, and K. S. Oh, Crit. Rev. Solid State **29**, 45 (2004).
[14]Y. K. Yan, K. H. Cho, and S. Priya, J. Am. Ceram. Soc. **94**, 1784 (2011).
[15]E. M. Sabolsky, G. L. Messing, and S. Trolier-McKinstry, J. Am. Ceram. Soc. **84**, 2507 (2001).
[16]T. Richter, S. Denneler, C. Schuh, E. Suvaci, and R. Moos, J. Am. Ceram. Soc. **91**, 929 (2008).
[17]S. J. Zhang, S. M. Lee, D. H. Kim, H. Y. Lee, and T. R. Shrout, J. Appl. Phys. **102**, 114103 (2007).
[18]S. J. Zhang, S. M. Lee, D. H. Kim, H. Y. Lee, and T. R. Shrout, Appl. Phys. Lett. **93**, 122908 (2008).
[19]M. Zgonik, P. Bernasconi, M. Duelli, R. Schlesser, P. Gunter, M. H. Garrett, D. Rytz, Y. Zhu, and X. Wu, Phys. Rev. B **50**(9), 5941 (1994).
[20]D. Liu, Y. K. Yan, and H. P. Zhou, J. Am. Ceram. Soc. **90**, 1323 (2007).
[21]K. H. Cho, C. S. Park, and S. Priya, Appl. Phys. Lett. **97**, 182902 (2010).